



How Can a Patient Blind to Radial Motion Discriminate Shifts in the Center-of-Motion?

SCOTT A. BEARDSLEY

*Department of Biomedical Engineering, Brain and Vision Research Laboratory, Boston University,
44 Cummington St., Boston, MA 02215, USA*

LUCIA M. VAINA*

*Department of Biomedical Engineering, Brain and Vision Research Laboratory, Boston University,
44 Cummington St., Boston, MA 02215, USA; Department of Neurology, Harvard Medical School,
75 Francis Street, Boston, MA 02215, USA*

vaina@bu.edu

Received March 5, 2004; Revised July 12, 2004; Accepted August 24, 2004

Action Editor: Kenneth D. Miller

Abstract. Within biologically constrained models of heading and complex motion processing, localization of the center-of-motion (COM) is typically an implicit property arising from the precise computation of radial motion direction associated with an observer's forward self-motion. In the work presented here we report psychophysical data from a motion-impaired stroke patient, GZ, whose pattern of visual motion deficits is inconsistent with this view. We show that while GZ is able to discriminate direction in circular motions she is unable to discriminate direction in radial motion patterns. GZ's inability to discriminate radial motion is in stark contrast with her ability to localize the COM in such stimuli and suggests that recovery of the COM does not necessarily require an explicit representation of radial motion direction. We propose that this dichotomy can be explained by a circular template mechanism that minimizes a global motion error relative to the visual motion input, and we demonstrate that a sparse population of such templates is computationally sufficient to account for human psychophysical performance in general and in particular, explains GZ's performance. Recent re-analysis of the predicted receptive field structures in several existing heading models provides additional support for this type of circular template mechanism and suggests the human visual system may have available circular motion mechanisms for heading estimation.

Keywords: computational modeling, neurological patient, optic flow, psychophysics, visual motion deficits

Perceptual information regarding heading (i.e., direction of self-motion), time to contact, object motion, depth, and scene segmentation can all be recovered to various degrees by analyzing the *motion components* (spiral, planar, etc.) comprising optic flow; for review see (Andersen, 1997; Vaina, 1998). These motion components can themselves be broken down into more ba-

sic properties (speed, direction, center-of-motion etc.) whose associated computational and neural mechanisms have been postulated to form the basis for the extraction of perceptually relevant information from the visual scene (Albright and Stoner, 1995; Cornilleau-Peres and Gielen, 1996; Duffy and Wurtz, 1995).

The extraction of heading from optic flow can, for example, be reduced to the ability of the visual system to localize the focus of expansion associated with the

*To whom all correspondence should be addressed.

observer's self-motion. Since, under natural conditions, the optic flow field generated by self-motion is only one component of a complex retinal flow field containing object, eye, and/or head motions, the computational task can be segregated into two distinct elements. The first involves the extraction of the observer's self-motion from the visual scene and the second requires localization of the corresponding focus-of-expansion, or more generally the center-of-motion (COM), associated with the observer's forward motion (Bruss and Horn, 1983; Gibson, 1950; Warren et al., 1988).

Within biologically constrained models of heading estimation, localization of the COM has typically been an implicit property arising from the global pattern of local *motion directions* to which a neuron is preferentially responsive (Cameron et al., 1998; Hatsopoulos and Warren, 1991; Perrone, 1992; Perrone and Stone, 1994; Zemel and Sejnowski, 1998). Computationally this template matching implementation seems reasonable given the wealth of psychophysical (Burr et al., 1998; Freeman and Harris, 1992; Meese and Harris, 2002; Morrone et al., 1995; Snowden and Milne, 1996) and neurophysiological (Anderson and Siegel, 1999; Duffy and Wurtz, 1991; Geesaman and Andersen, 1996; Graziano et al., 1994; Schaafsma and Duysens, 1996; Siegel and Read, 1997) data supporting the existence of specialized detectors for the motion pattern components (e.g., radial and spiral motions) typically encountered during self-motion through a rigid environment. In such "motion template" models heading is estimated by identifying the template whose motion pattern most directly matches the motion within the visual scene. Under these conditions, localization of the COM for heading is directly tied to the wide-field *radial* structure of the local motion directions associated with an observer's forward self-motion.

In the work presented here we report psychophysical data from a motion-impaired stroke patient, GZ (Vaina and Rushton, 2000), that is at odds with the generally accepted view that precise computation of radial motion direction within optic flow is necessary to recover the COM associated with self-motion (Bruss and Horn, 1983; Rieger and Lawton, 1985). The pattern of GZ's visual motion deficits suggests that localization of the COM need not be based on radial templates matched to specific heading trajectories, but may instead be mediated by a *circular* template mechanism whose computational structure is insensitive to gross changes in radial motion direction (e.g. expansion vs. contraction) but is tightly coupled to the deviations in local motion

direction inherent in shifting the radial COM. Together with the development of a computational model that minimizes a global circular motion error relative to the visual motion input, we demonstrate that a sparse population of circular templates is computationally sufficient to spatially localize the COM and account for GZ's psychophysical performance. Such circular template mechanisms have been proposed to play a role in estimating heading (Beintema and van den Berg, 1998; Beintema et al., 2004) and together with the results presented here suggest that the human visual system may have available circular motion mechanisms for processing self-motion.

Material and Methods

Observers

In total, 27 normal right-handed observers (not including patient GZ) participated in the psychophysical tasks: 16 in the motion pattern coherence task and 11 in the shifted center-of-motion (COM) task. All observers had normal or corrected to normal vision. Prior to participation in the study written informed consent was obtained from all subjects in accordance with Boston University's Institutional Review Board Committee on research involving human subjects.

Motion Pattern Coherence Task

In the motion pattern coherence task observers were required to discriminate the direction of radial (expansion vs. contraction) or circular (clockwise (CW) vs. counter-clockwise (CCW) rotation) motion formed by a proportion of coherently moving 'signal' dots. Within each motion sequence dots were randomly assigned as 'signal' or 'noise' on a frame-by-frame basis such that signal dots moved with a velocity of 3°/s in directions consistent with the motion pattern being presented and noise dots were randomly repositioned within the stimulus aperture (Fig. 1(a)). Across the population of dots, this resulted in a decreasing probability of uninterrupted local motion for the i th dot (d_i)

$$P(d_i) = \left[\frac{C_p}{100\%} \right]^n$$

that was a function of the motion pattern coherence (C_p), i.e, proportion of signal to noise dots, and the number of consecutive signal frames (n).

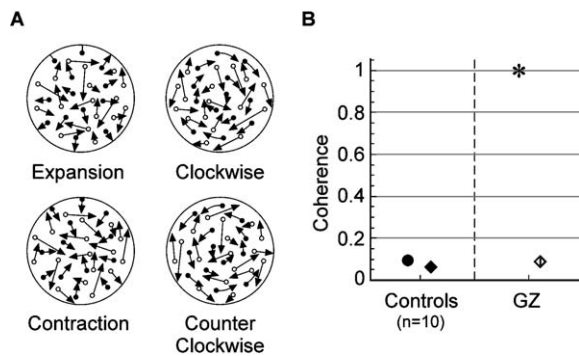


Figure 1. Motion pattern coherence task. (A) In a single interval task, observers were required to discriminate the direction of radial (expansion vs. contraction) or circular (clockwise vs. counter-clockwise rotation) motion formed by a proportion of coherently moving ‘signal’ dots. Within each motion sequence dots were randomly assigned as ‘signal’ or ‘noise’ on a frame-by-frame basis such that signal dots moved in directions consistent with the motion pattern being presented and noise dots were randomly repositioned within the stimulus aperture. (B) Motion pattern coherence thresholds (\pm SD) for radial (circles) and circular (diamonds) motions. Seven months after the lesion GZ remained unable to discriminate direction in radial motions (asterisk), consistently performing at chance across a wide range of speeds (3–30°/sec), even for stimuli containing fully coherent motion. In contrast, her ability to discriminate direction in circular motions (open diamond) was normal for stimuli presented with central fixation (Difference = 2.22% < $2\sigma_{\text{controls}}$).

Each motion sequence was presented for 880 ms (22 frames; 40 ms per frame) and consisted of a dynamic random dot display containing 157 white dots presented on a black background (79.2 and 3.9 Cd/m² respectively) and uniformly distributed within a 10°

circular aperture (54 cm viewing distance). All stimuli were presented on a 17" Apple Studio Display monitor with a screen resolution and refresh rate of 832 × 624 pixels and 75 Hz respectively.

For each observer and class of motions, radial and circular, discrimination thresholds were obtained for stimuli presented with central fixation. Within a test session, discrimination thresholds for opposing motions (e.g., expansion vs. contraction) were measured as a function of the stimulus coherence using a single interval adaptive staircase paradigm. Thresholds within each staircase were estimated at the 79% criterion as the mean over the last six reversals within the 3-down, 1-up phase of the paradigm.

Shifted Center-of-Motion (COM) Task

In the shifted center-of-motion (COM) task, observers were presented with pairs of expanding or contracting motions whose COM was shifted to the left and right of a central fixation (Fig. 2(a)). For each pair of motion pattern stimuli (expansion or contraction), the COM was shifted within the central 4° formed by an *illusory* inner stimulus aperture and the observer’s task was to select the stimulus whose COM was shifted to the right of the central fixation marker. Since the COM was not explicitly visible during presentation, observers were forced to infer its position by integrating the local dot trajectories across the global motion pattern.

Stimuli consisted of a dynamic random dot display containing 190 uniformly distributed dots presented within a 24° diameter annular region (central 4°

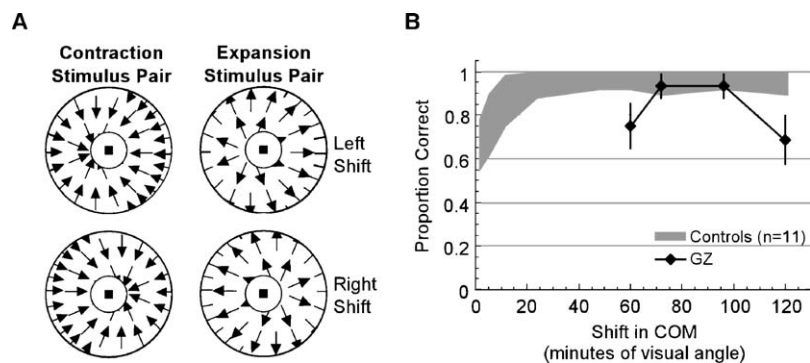


Figure 2. Shifted center-of-motion (COM) task. (A) Schematic representation of the shifted COM task for radial motions. Stimuli consisted of coherent expanding or contracting dynamic random dot displays presented in a 24° annular region, with the central 4° removed. In a 2-TAFC task observers were required to select the stimulus whose COM was shifted to the right of a central fixation (filled square). (B) COM discrimination for radial motions. GZ’s proportion correct (\pm SD) across constant stimulus levels (diamonds) is plotted against the range in performance recorded across eleven normal observers (shaded region). While GZ’s performance remained greater than chance across the constant stimulus levels tested, her ability to discriminate small shifts (1–2°) in the COM was somewhat impaired relative to controls.

removed) on a gray background (5.2 Cd/m^2). All stimulus apertures were *illusory* as defined by an absence of dots.

Stimuli were generated off-line and presented on a 17" Apple Studio Display monitor at a 54 cm viewing distance with a screen resolution and refresh rate of 832×624 pixels and 75 Hz respectively. Dot luminance was set to 9.3 Cd/m^2 to reduce static cues associated with phosphor relaxation across successive screen refreshes while maintaining contrast at supra-threshold levels (i.e., 28%).

At the subject viewing distance each dot subtended 9.8 minutes of visual angle and moved through a radial speed gradient whose maximum speed at the outer stimulus aperture was $43.9^\circ/\text{sec}$. All dots moved coherently with an average dot speed of $30^\circ/\text{sec}$ in directions consistent with the global motion pattern being presented (i.e., expansion or contraction) and uniform dot density was actively maintained throughout the stimulus presentation (Clifford et al., 1999). Dot lifetimes were limited to eleven frames (147 ms) and coherent flicker associated with dot replacement was minimized by uniformly distributing the initial dot lifetimes among the first eleven frames.

During the task, stimulus duration was randomly set to one of seven discrete values, spanning the range 33 ± 3 frames, to minimize the use of local dot displacements within the speed gradient as a cue to localize the center-of-motion. Across trials, this resulted in a pseudo-random stimulus duration spanning the range 440 ± 40 ms.

Discrimination for the magnitude of the COM shift was quantified using a two-temporal alternative forced choice constant stimulus paradigm. Within each test session observers were presented with pairs of pseudo-randomly interleaved expanding and contracting motion patterns (500 ms inter-stimulus interval). Percent correct performance for the temporal order of each left-right shifted stimulus pair was measured as a function of the shift in the COM across four randomly interleaved constant stimulus levels (128 stimuli per session).

Discrimination thresholds for normal observers were calculated at the 82% criterion for each constant stimulus session using a least-squares Weibull fit to the psychometric function estimated across constant stimulus levels. A χ^2 goodness-of-fit was calculated for each psychometric function to exclude data sets with poor curve fits from further analysis ($\chi^2(v) < \chi_R^2(v)$; $p < 0.05$), where $\chi_R^2(v)$ is the rejection criterion ($p <$

0.05) for a data set containing (v) degrees of freedom (Bevington, 1969). For each observer, expansion and contraction thresholds were averaged separately across 3–7 constant stimulus sessions to quantify the difference in COM discrimination between opposing motion patterns.

Circular Template Model

During observer motion, the corresponding motion of a point (X, Y, Z) in the external environment can be instantaneously described by three translational (T_x, T_y, T_z) and three rotational ($\Omega_x, \Omega_y, \Omega_z$) components of motion defined along the X, Y , and Z axes relative to the observer. For an image plane located a focal distance (f) from the observer, the projective transformation of each point (X, Y, Z) from 3-D space into the 2-D (x, y) image plane is given by

$$x = f \frac{X}{Z}, \quad y = f \frac{Y}{Z}$$

The corresponding projection of the observer's 3-D motion is given by the optic flow field $V = (u, v)$

$$\begin{aligned} u(x, y) &= \frac{-fT_x + xT_z}{Z} + \frac{xy}{f}\Omega_x \\ &\quad - \left(f + \frac{x^2}{f}\right)\Omega_y - y\Omega_z \\ v(x, y) &= \frac{-fT_y + yT_z}{Z} \\ &\quad + \left(f + \frac{y^2}{f}\right)\Omega_x - \frac{xy}{f}\Omega_y - x\Omega_z \end{aligned}$$

where $u(x, y)$ and $v(x, y)$ correspond to the x - and y -components of the image motion at the point (x, y), (Longuet-Higgins et al., 1980). In this formulation, the location of the COM associated with the observer's translational motion corresponds to the direction of heading and is given by the point ($\tau = fT_x/T_z, \eta = fT_y/T_z$).

From the expressions for $u(x, y)$ and $v(x, y)$ it is clear by inspection that $V(x, y)$ can be decomposed into a sum of two vector fields associated with the translating $V_T(x, y)$ and rotating $V_\Omega(x, y)$ components of the observer's self-motion:

$$V(x, y) = V_T(x, y) + V_\Omega(x, y)$$

Since the direction of self-motion, (τ, η), is uniquely specified by the translational components of the observer's motion, the task of estimating heading can

be reduced to one of localizing the COM associated with the velocity field $V_T(x, y)$ under conditions in which (a) the rotational components of the observer's motion $V_\omega(x, y)$ have been segmented from the optic flow or (b) when there is no rotational motion, $V_\omega(x, y) = 0$.

If we define a series of circular templates within the visual field parameterized only by the locations of their centers-of-motion (x_0, y_0) such that the local template motion at any point is given by

$$(-y + y_0, x - x_0)$$

then the COM of the optic flow can be localized by computing a generalized scalar function whose norm is quadratic in terms of x_0 and y_0 (Sundaeswaran, 1992). For a circular template sampling an arbitrary optic flow, we can define the scalar product $U(x, y)$ across all locations in the image plane such that

$$\begin{aligned} U_{(x_0, y_0)}(x, y) &= V(x, y) \cdot (-y + y_0, x - x_0) \\ &= V_T(x, y) \cdot (-y + y_0, x - x_0) \end{aligned}$$

$$\begin{aligned} &+ V_\Omega(x, y) \cdot (-y + y_0, x - x_0) \\ &= U_{(x_0, y_0)}^T(x, y) + U_{(x_0, y_0)}^\Omega(x, y) \end{aligned}$$

where $U_{(x_0, y_0)}^T(x, y)$ and $U_{(x_0, y_0)}^\Omega(x, y)$ correspond to the translational and rotational components of the scalar product for the circular template whose COM is located at (x_0, y_0) . By definition the scalar product will be zero when all local motion points are mutually orthogonal to the circular template.

For simple radial motions presented during fixation, such as those used in the shifted COM task, no rotational motion components are present in the resulting optic flow (i.e., $V_\Omega(x, y) = 0$). Under these conditions the local motions of a circular template will be mutually orthogonal to the underlying radial motion only when the stimulus and template centers-of-motion coincide (Fig. 3(a)).

If we define a scalar error, $E(x_0, y_0)$, calculated across circular template locations (x_0, y_0) such that

$$\begin{aligned} E(x_0, y_0) &= \|U_{(x_0, y_0)}(x, y)\|^2 \\ &= \|U_{(x_0, y_0)}^T(x, y)\|^2, \quad \text{when } V_\Omega(x, y) = 0 \end{aligned}$$

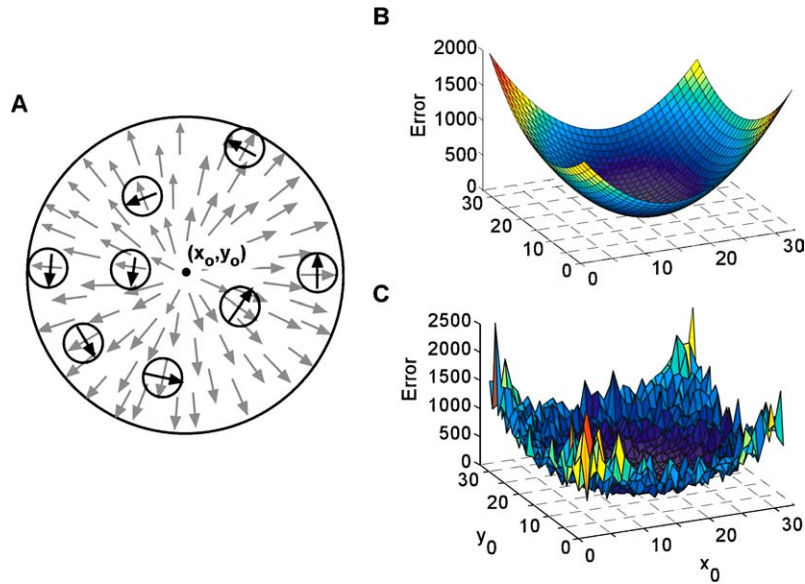


Figure 3. Circular template model (A) Schematic example of a circular template sampling eight locations (small circles) of an expanding motion pattern in which the template center (x_0, y_0) and the stimulus COM coincide. At each location the local motion of the circular template (black arrows) is orthogonal to the local motion in the stimulus (gray arrows). (B) Error surface, $E(x_0, y_0)$, resulting from a uniformly distributed population of circular templates, parameterized by their centers (x_0, y_0) , where each template samples the *same set* of motion locations in the stimulus (Sundaeswaran, 1992). By definition, the global minimum corresponds to the circular template whose local vectors are most orthogonal to the stimulus motion, which occurs when the template center and stimulus COM coincide. (C) Error surface for the circular template model simulated here. In the model each template samples a *different set* of randomly chosen motion locations in the stimulus. Together with the presence of radial speed gradients in both the stimulus and the circular templates the random selection of local motions introduced a multiplicative noise whose magnitude is proportional to the template error, $E(x_0, y_0)$. As in (B), $E(x_0, y_0)$ contains a single global minimum corresponding to the template whose center coincides with the stimulus COM.

then $E(x_0, y_0)$ is associated *only* with the translational component of the scalar product, $U_{(x_0, y_0)}^T$, when $V_\Omega(x, y) = 0$. It can be shown that since $U_{(x_0, y_0)}^T$ is a function only of (x_0, y_0) the resulting error surface $E(x_0, y_0)$ is quadratic such that it contains a single (global) minimum (Fig. 3(b)). Since, by definition, the global error minimum corresponds to the circular template most orthogonal to the stimulus motion, its location (x_0, y_0) within the template space can be used to estimate the location of the stimulus COM.

Simulating the Shifted COM Task—Circular Template Model

To test the model's performance on the shifted COM task, vector field representations of the shifted radial motion stimuli were presented to the model. Each stimulus consisted of 190 motion vectors randomly positioned in an annular stimulus window whose outer aperture was inscribed within a 32×32 vector field of image locations (x, y) . To prevent resolution artifacts associated with the reduced number of image locations (relative to the 832×624 screen resolution in the psychophysical task), the location of the COM was continuously valued within the simulated stimulus and thus was not constrained to correspond to specific image locations. Unless otherwise specified the direction and speed (i.e., magnitude) of each motion vector were consistent with the type of shifted motion pattern being presented. All other matrix locations were zero.

The model consisted of a sparse population of 54 circular templates whose centers (x_0, y_0) were randomly distributed across the 32×32 grid of possible image locations (x, y) . Each template consisted of a 32×32 vector field containing nonzero vectors given by $(-y + y_0, x - x_0)$ for all image locations contained within the stimulus annulus. For each stimulus the error $E(x_0, y_0)$, associated with the template (x_0, y_0) , was calculated as the scalar product between N randomly chosen nonzero stimulus motion vectors and their corresponding template vectors. For each stimulus, the spatial location of the COM was estimated from the resulting error surface using a least-squares estimate of the global error minimum obtained across the template population (Fig. 3(c)).

Equivalent measures of perceptual performance were obtained from the model using the procedures outlined in the psychophysical task by comparing COM estimates between left/right shifted stimulus pairs. For

each left/right shifted stimulus pair, the model's performance was judged to be correct if $x_{\text{left shift}} < x_{\text{right shift}}$. As with the psychophysical task, discrimination thresholds (82% criterion) were estimated from a least-squares fit to the psychometric function measured using a constant stimulus paradigm.

Where indicated in the simulations, motion noise was incorporated into the stimulus by pseudo-randomly perturbing the angle of each motion vector over the range $[-\theta_p, \theta_p]$ degrees centered on the local direction defined by the shifted radial motion pattern. Under these conditions the error surface, $E(x_0, y_0)$, was not constrained to be locally smooth due to the random sampling of image locations across the template population. In conjunction with the radial speed gradients present in both the stimulus and circular templates the pseudo-random perturbation of local motion directions introduced a multiplicative noise whose variance was proportional to the template error (Fig. 3(c)).

Computationally the resulting "noise" in the system reflects errors in the local motion information projected to the circular templates. Perceptually, such noise could result from internal sources associated with the estimation of local motion direction and/or external sources associated with the composition of the stimulus itself.

Results

Patient GZ is a 67 year-old right-handed woman with a large bilateral infarct involving the right occipital lobe and the parietal areas 7a and 7b bilaterally. The right hemisphere lesion involved the MT-complex. GZ presented with severe motion discrimination deficits and her distance and depth perception (both global and local stereopsis) were also very impaired. Initially she was unable to make tracking or saccadic eye movements on command (although her spontaneous eye movements were normal), but neuro-ophthalmological evaluations repeated at six and seven months after the stroke indicated full recovery. At that time her visual fields were full in the central 25° . After seven months of weekly testing and retraining sessions GZ's spatial discrimination and low-level direction discrimination recovered, yet her depth perception remained severely impaired as was her ability to discriminate speed and the direction of radial motion patterns. GZ was, however, able to discriminate planar motion attributes, such as direction of frontoparallel translation or rotation.

Discriminating Radial and Circular Motion Patterns

Figure 1 illustrates GZ's threshold performance (\pm SD) relative to a control group of normal observers seven months after her lesion. Across normal observers, coherence thresholds for circular motions remained significantly lower than radial motions ($p < 0.005$, $t(18) = 3.17$). After seven months, GZ remained unable to discriminate direction in radial motions, consistently failing the task across a wide range of speeds (3–30°/sec), even for stimuli containing fully coherent motion. In contrast, her ability to discriminate direction in circular motions was normal for stimuli presented with central fixation (Difference = 2.22% $< 2\sigma_{\text{controls}}$).

This dissociation between radial and circular motions is intriguing, particularly when considered in the context of the neurophysiological and cortical mechanisms believed to underlie motion pattern processing. In both cases, the same cortical areas have been shown to subserve radial and circular motion processing (Anderson and Siegel, 1999; Bremmer et al., 2002; Duffy and Wurtz, 1991; Geesaman and Andersen, 1996; Graziano et al., 1994; Morrone et al., 2000; Schaafsma and Duysens, 1996; Siegel and Read, 1997). In the context of GZ this would suggest that she should be able to discriminate both radial and circular motions, or neither.

It could be argued that GZ's poor depth perception contributed to the dissociation between radial and circular motions. Certainly there are reports in the literature arguing that radial, but not circular, motion conveys an illusion of depth, which may play some role in its discrimination (Bex and Makous, 1997). However, such effects tend to be modulatory (Clifford et al., 1999), and more importantly as we show below, cannot account for GZ's ability to discriminate shifts in the COM for which the depth illusion is constant.

Discriminating Shifts in the COM for Radial Motions

In a second series of visual motion tasks, GZ's ability to spatially localize the radial COM in a central fixation display was quantified using an interleaved constant stimulus paradigm to estimate percent correct performance for each of four COM shifts (60, 72, 96, and 120 arcmin). A control group of normal observers was tested across a matched range of constant stimulus levels that was subsequently extended to estimate thresh-

old performance (2.4–120 arcmin across eight constant stimulus levels).

Across observers, discrimination thresholds (\pm SE) for expanding and contracting motions were 10.27 ± 1.41 and 7.85 ± 1.07 minutes of visual angle respectively ($n = 11$). While thresholds for contracting motions were generally lower than those for expanding motions the difference across observers was not statistically significant ($p > 0.1$, $t(20) = 1.36$).

For small shifts in the COM (60–120 arcmin), GZ's ability to discriminate the direction of shifts (left vs. right) remained greater than chance across constant stimulus levels¹ (Fig. 2(b)). While it is clear from the group averaged radial performance that GZ's ability to discriminate small shifts was somewhat impaired, the fact that she could perform the task at all is significant in light of her inability to discriminate gross directions in fully coherent radial motion patterns (i.e., expansion vs. contraction).

Within the context of existing motion pattern and heading mechanisms the apparent dichotomy in GZ's radial motion discrimination versus her ability to localize the COM is a challenge to explain. The implicit assumption that COM localization is directly coupled with precise computation of the *radial direction* information (Cameron et al., 1998; Hatsopoulos and Warren, 1991; Perrone, 1992; Perrone and Stone, 1994; Zemel and Sejnowski, 1998), suggests that such localization should be severely impaired in individuals who have lost the ability to differentiate gross changes in radial motion direction (e.g., expansion vs. contraction). However, as GZ's performance indicates, this need not be the case.

Given the relatively large shifts in the COM presented to GZ, with respect to normal observer thresholds, it could be argued that GZ makes use of local motion mechanisms to localize the COM, essentially performing a direction discrimination task within limited regions of the visual field. However, if this were the case we would expect her performance on the motion pattern coherence task, for which the direction differences in the local signal motion are maximized (i.e., Fig. 2; expansion vs. contraction), to be either 100% (i.e., normal) or 0% (inverted judgments). This did not occur. GZ's ability to discriminate expansion from contraction was at chance for fully coherent stimuli.

Alternatively, the radial speed gradient might be used to discriminate shifts in the COM without requiring specific direction information. Under these conditions

the direction of shift could be determined globally by identifying the visual field (right or left) containing the slower average dot speed or locally by identifying the location of the lowest speed in the region around the inner stimulus aperture. Tests of normal observers using stimuli that systematically controlled for the presence of motion direction or speed gradient information indicate that speed does not provide a strong cue during the task. Across observers, shifted COM thresholds for radial motions increased significantly when only the speed gradient information was present (i.e., random motion directions), ($p < 0.05$; $t(10) = 3.86$), and actually decreased or showed no significant change when the speed gradient was removed, ($p \geq 0.025$; $t(10) \leq 2.19$ —data not shown). In the latter condition both the global structure of motion directions and temporal distribution of speeds was maintained. In the case of GZ, the utilization of such speed cues is further compromised by her inability to discriminate speed during the time the COM test was administered (seven months after the lesion).

Circular Template Model

Based on the pattern of GZ's visual deficits, and her ability to discriminate circular motions, we propose that a circular template mechanism may be utilized by the visual system to localize the radial COM. Computationally similar mechanisms have been shown to extract robust estimates of heading in computer vision systems (Hummel and Sundaeswaran, 1993; Sundaeswaran, 1992) and more recently in biologically inspired models of heading (Beintema and van den Berg, 1998; Beintema et al., 2002; Beintema et al., 2004), and together with the presence of circular-tuned cells in the visual cortex, provide a computational and neurophysiological foundation upon which such a system might be based. Here we outline the basic computational structure for such a mechanism and demonstrate that it (a) does not require an implicit mechanism to discriminate radial motion and (b) is computationally sufficient to account for COM discrimination.

An underlying premise behind the use of circular motion templates is the observation that the optic flow field $V(x, y)$ resulting from an observer's self-motion can be decomposed into translational ($V_T(x, y)$) and rotational ($V_\omega(x, y)$) components associated with the observer's translation and head/eye rotations respectively (Longuet-Higgins et al., 1980). Within this rep-

resentation, the computational task of recovering the observer's heading can be reduced to one of spatially localizing the COM associated with the velocity field $V_T(x, y)$ under conditions in which (a) the rotational components of the observer's motion $V_\omega(x, y)$ have been segmented from the optic flow or (b) when there is no rotational motion, $V_\omega(x, y) = 0$.

For simple radial motions presented during fixation, such as those used in the shifted COM task, no rotational motion components are present ($V_\omega(x, y) = 0$). Under these conditions the local motions of a circular template will be mutually orthogonal to the underlying radial motion only when the stimulus and template centers-of-motion coincide (Fig. 3(a)). Across a population of templates parameterized by their centers-of-motion (x_0, y_0) , the resulting error surface $E(x_0, y_0)$ is quadratic in form such that it contains a single (global) minimum, (Fig. 3(b) and (c)). Since the global error minimum corresponds to the circular template most orthogonal to the stimulus motion, its location within the template space (x_0, y_0) can be taken as an estimate of the stimulus COM (Hummel and Sundaeswaran, 1993; Sundaeswaran, 1992).

To examine the computational sufficiency of this approach, we simulated the COM task across a sparse population of circular motion templates pseudo-randomly spaced throughout the visual field. In a series of simulations we systematically varied the density of circular templates, the number of motion points sampled by each template, and perturbations in the local stimulus motion to quantify the limits of the model's performance and its robustness under more biologically plausible conditions.

The model's grouped threshold performance on the COM task is shown in Fig. 4(a) for radial motions. Discrimination thresholds were averaged across five simulations and are shown here as a function of the number of sampled motion points within each template [4, 28] and the degree of local motion perturbation [0, 44] for a sparse population containing 54 circular templates. Similar trends in threshold performance were observed for expanding and contracting stimuli individually and with larger template populations. For templates receiving accurate local motion estimates and sampling a moderate number of motion points (e.g., 28), COM thresholds were consistent with human observers (Fig. 4(a)—lower left corner). This can be seen more clearly in the plot of threshold performance versus local motion perturbation (Fig. 4(b)). For 28 sample points the averaged COM threshold for radial motions

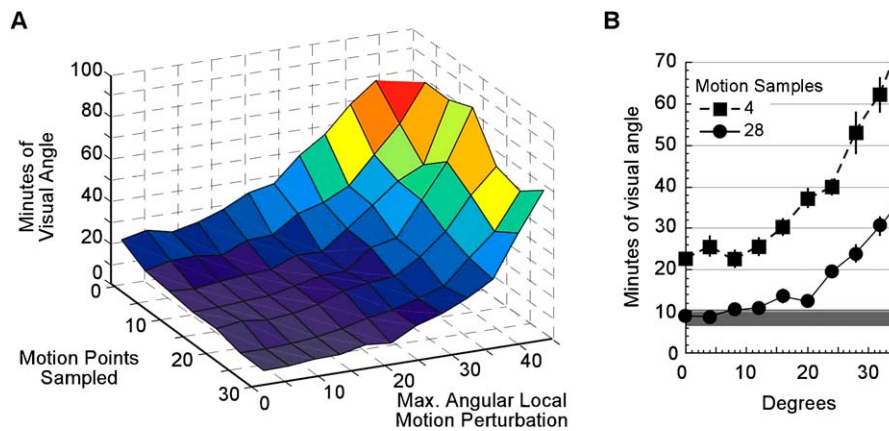


Figure 4. Circular template model performance on the shifted COM task. (A) COM thresholds (averaged across five simulations) for radial motions as a function of the number of sampled motion points and the degree of local motion perturbation. For templates receiving accurate local motion estimates and sampling a moderate number of motion points (e.g., 28), discrimination thresholds were consistent with human observers ($p = 0.59$, $t(19) = 0.24$). As local motion estimates became less accurate the model's performance systematically degraded, however, even for relatively large deviations in the local motion estimates (e.g., ± 20 deg.) the model's ability to localize the stimulus COM remained robust. (B) COM thresholds (\pm SE) for radial motions as a function of the degree of local motion perturbation for templates sampling four (square) and 28 (circle) motion points respectively. For comparison, the shaded region indicates the average radial COM threshold (\pm SE), (3–7 estimates per observer for each radial motion) across 11 normal observers. For circular templates sampling 28 motion points under low noise conditions (consistent with the original psychophysical task), the averaged COM threshold, 8.76 ± 0.86 minutes of visual angle, was well-matched to that for normal observers (9.06 ± 0.88 arcmin).

under no noise conditions (8.76 ± 0.86 arcmin) was not significantly different from human observers ($p = 0.59$, $t(19) = 0.24$). As the motion sampling density decreased the model's performance remained robust, yielding thresholds consistent with human observers for as few as eight sampled motion points per template under low noise conditions.

Similar trends in performance were observed as the accuracy of the local motion estimates was reduced, however, even for relatively large deviations in the local motion estimates (e.g., ± 20 deg.) the model's ability to localize the stimulus COM remained robust. Figure 5 shows the equivalent percent correct performance as a function of the degree of COM shift for the circular template model. Performance is plotted for two sets of sampled motion points (4 and 28 samples) and two levels of local motion noise (0 and 32° perturbation) to provide a more direct comparison of the model's performance relative to GZ and normal observers. For small motion samples (i.e., four points per template) containing moderate error in the local motion estimates (± 16 – 32 deg.) the trend in the model's performance was qualitatively similar to that reported for GZ, while for low noise and/or moderate sampling conditions, the model's performance was well matched to that of normal observers.

Discussion

We have identified a stroke patient, GZ, whose pattern of visual motion deficits is inconsistent with the conventional view that localization of the center-of-motion (COM) in complex visual displays requires the use of radial motion mechanisms. We have shown that while GZ is able to discriminate direction in circular motion displays she is unable to do so for radial motions. Even more intriguing than GZ's total inability to discriminate direction in radial motions is the fact that it *did not* prevent her from localizing the COM contained within those motion patterns. This dissociation between her ability to discriminate the types of radial motion and the location of the COM is at odds with the generally accepted view that a precise computation of local and/or global radial motion information is necessary to recover the COM (Bruss and Horn, 1983; Rieger and Lawton, 1985).

We propose that this dichotomy can be explained by a circular template mechanism that minimizes a global motion error relative to the visual motion input. By its nature the circular template model proposed here does not require an implicit mechanism to discriminate the direction of radial motion. The use of globally orthogonal motion templates that effectively

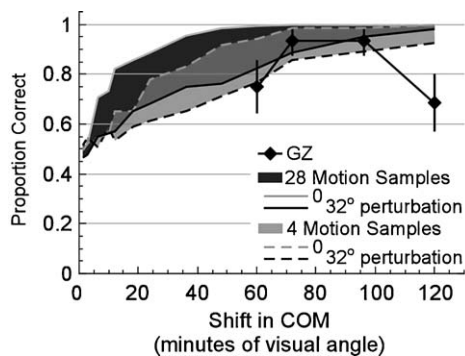


Figure 5. Percent correct discrimination as a function of COM shift for the circular template model. Performance is plotted for two sets of sampled motion points (4 and 28 samples) and two levels of local motion noise (0 and 32° perturbation) to provide a more direct comparison of the model's performance relative to GZ and normal observers. Performance for intermediate levels of motion perturbation (not shown) systematically spanned the shaded regions (light gray and black—4 and 28 motion samples per template respectively; dark gray—overlap in performance). Under low sampling conditions containing moderate error in the local motion estimates (i.e., 32°) the trend in the model's performance was qualitatively similar to that reported for GZ. For templates receiving a moderate number of low noise motion inputs, the model's performance was well matched to that of normal observers.

seek to maximize local motion differences relative to the visual input results in a computational mechanism capable of localizing the COM without the need to differentiate the type of radial motion present. As we have shown in a series of simulated psychophysical tasks this type of mechanism is computationally sufficient to account for human psychophysical performance in general and in particular, explains GZ's performance.

The circular template mechanism outlined here is quantitatively similar to the retinal flow templates proposed previously by Beintema and colleagues in their velocity gain field model (Beintema and van den Berg, 1998; Beintema et al., 2004). In their model, rotation tuned retinal motion templates perform an inner product computation to evaluate the similarity between the observed flow and the template's preferred self-motion. Invariance to eye rotations was obtained in a second stage by combining the responses of retinal flow templates with extra retinal eye velocity signals to create head-centric templates tuned to specific instances of heading. Similar computational mechanisms could be included in the model proposed here to account for the more generalized case of self-motion in the presence of eye-movements.

Recent analyses of the predicted receptive field structures in the population model of heading proposed by Lappe and Rauscheker (1993, 1995) and Perrone and Stone's template model (1992, 1994) provide additional support for the type of circular templates proposed here (Beintema et al., 2002; Beintema et al., 2004), and together with the original models suggests a neurophysiological locus in MSTd. Although the anatomical locus of GZ's lesion does not necessarily preclude a similar interpretation in the case of MSTd, the strong representation of radial tuning in MSTd coupled with GZ's inability to discriminate radial motions, suggests that alternate neural structures may be used to localize the COM.

Given the wide range of cortical areas known to be responsive to optic flow (Anderson and Siegel, 1999; Duffy and Wurtz, 1991; Geesaman and Andersen, 1996; Graziano et al., 1994; Morrone et al., 2000; Schaafsma and Duysens, 1996; Siegel and Read, 1997), the existence of alternate processing pathways seems plausible. For example, "flow general" neurons in area 7a have been shown to be selective for the class of motion, i.e., radial or circular motion (Siegel and Read, 1997), and would seem ideally suited to the task. While the extent of GZ's lesion would seem to rule out involvement of area 7a in the perceptual tasks, there is evidence suggesting the presence of flow general neurons in other cortical areas such as the anterior superior temporal polysensory area (STPa), (Anderson and Siegel, 1999), that are not directly involved in GZ's lesion.

Alternatively, pairs of neurons tuned to opposing types of rotation (e.g., clockwise or counterclockwise) could be combined to compute a bi-directional global motion error. Computationally, this approach is equivalent to the difference operations performed among bi-circular templates in the velocity gain field model to compensate for eye movements (Beintema and van den Berg, 1998; Beintema et al., 2002; Beintema et al., 2004). Such mechanisms are consistent with the presence of rotation selective neurons in cortical areas responsive to optic flow, however as we have noted previously, the co-commitment representation of radial motions in these areas would seem to be at odds with the radial/circular dissociation reported in GZ.

Conceptually, the use of circular mechanisms to localize the radial COM seems counter-intuitive. However, in terms of practical applications, such as an observer estimating his/her direction of self-motion (i.e., heading), the existence of such mechanisms is

computationally appealing. Simple circular mechanisms, such as those proposed here, could be used to detect small spatial shifts in the COM associated with the change in direction of an observer's self-motion (Cavalleri et al., 2003). More complex forms, such as the bi-circular mechanisms posited by Beintema and colleagues (Beintema et al., 2002; Beintema et al., 2004), could be used to provide visual estimates of the global rotational motion components associated with eye and/or head movements while maintaining sensitivity to changes in the direction of self-motion. In both cases, the global minimization of scalar error with respect to what is effectively the translational component of the observer's self-motion results in heading estimates that are largely independent of the observer's speed and the relative depth of points in the scene, suggesting this type of circular mechanism as a useful way for recovering heading in more complex visual scenes.

Acknowledgments

This work was supported by NIH grant EY-2R01-07861-13 and NSF-SGR 0087198 to L.M.V.

Note

1. Although the decrease in GZ's performance with shifts of 120 arcmin was statistically significant ($p = 0.0017$), in our experience patients often make errors not directly associated with task difficulty (e.g., changes in attention), that can affect the statistical interpretation for small sample sizes such as those reported here (GZ; 16 trials per COM shift).

References

- Albright TD, Stoner GR (1995) Visual motion perception. *Proc. Natl. Acad. Sci. U.S.A.* 92: 2433–2440.
- Andersen RA (1997) Neural mechanisms of visual motion perception in primates. *Neuron* 18: 865–872.
- Anderson KC, Siegel RM (1999) Optic flow selectivity in the anterior superior temporal polysensory area, STPa, of the behaving monkey. *J. Neurosci* 19: 2681–2692.
- Beintema JA, van den Berg AV (1998) Heading detection using motion templates and eye velocity gain fields. *Vision Res.* 38: 2155–2179.
- Beintema JA, van den Berg AV, Lappe M, eds. (2002) Receptive field structure of flow detectors for heading perception. *Advances in Neural Information Processing Systems 14*. MIT Press, Cambridge, MA.
- Beintema JA, van den Berg AV, Lappe M (2004) Circular receptive field structures for flow analysis and heading detection. In: LM Vaina, SA Beardsley, SK Rushton, eds. *Optic Flow and Beyond*. Kluwer Academic Publishers, Dordrecht, pp. 223–248.
- Bevington PR (1969) *Data reduction and error analysis for the physical sciences*. McGraw-Hill Book Company, New York.
- Bex PJ, Makous W (1997) Radial motion looks faster. *Vision Res.* 37: 3399–3405.
- Bremmer F, Duhamel JR, Ben Hamed S, Graf W (2002) Heading encoding in the macaque ventral intraparietal area (VIP). *Eur. J. Neurosci.* 16: 1554–1568.
- Bruss AR, Horn BKP (1983) Passive navigation. *Comp. Vis. Graph. Image Proc.* 21: 3–20.
- Burr DC, Morrone MC, Vaina LM (1998) Large receptive fields for optic flow detection in humans. *Vision Res.* 38: 1731–1743.
- Cameron S, Grossberg S, Guenther FH (1998) A self-organizing neural network architecture for navigation using optic flow. *Neural Comput.* 10: 313–352.
- Cavalleri P, Sabatini SP, Solari F, Bisio GM (2003) Centric-minded templates for self-motion perception. *Vision Res.* 43: 1473–1493.
- Clifford CWG, Beardsley SA, Vaina LM (1999) The perception and discrimination of speed in complex motion. *Vision Res.* 39: 2213–2227.
- Cornilleau-Peres V, Gielen C (1996) Interactions between self-motion and depth perception in the processing of optic flow. *Trends Neurosci.* 19: 196–202.
- Duffy CJ, Wurtz RH (1991) Sensitivity of MST neurons to optic flow stimuli. I. A continuum of response selectivity to large-field stimuli. *J. Neurophysiol.* 65: 1329–1345.
- Duffy CJ, Wurtz RH (1995) Response of monkey MST neurons to optic flow stimuli with shifted centers of motion. *J. Neurosci.* 15: 5192–5208.
- Freeman TC, Harris MG (1992) Human sensitivity to expanding and rotating motion: Effects of complementary masking and directional structure. *Vision Res.* 32: 81–87.
- Geesaman BJ, Andersen RA (1996) The analysis of complex motion patterns by form/cue invariant MSTd neurons. *J. Neurosci.* 16: 4716–4732.
- Gibson JJ (1950) *The Perception of the visual world*. Houghton Mifflin, Boston, MA.
- Graziano MS, Anderson RA, Snowden RJ (1994) Tuning of MST neurons to spiral motions. *J. Neurosci.* 14: 54–67.
- Hatsopoulos NG, Warren WH (1991) Visual navigation with a neural network. *Neural Netw.* 4: 303–317.
- Hummel R, Sundaeswaran V (1993) Motion parameter estimation from global flow field data. *IEEE Trans. Pat. Anal. Mach. Intel.* 15: 459–476.
- Lappe M, Rauschecker JP (1993) A neural network for the processing of optic flow from ego-motion in man and higher mammals. *Neural Comput.* 5: 374–391.
- Lappe M, Rauschecker JP (1995) Motion anisotropies and heading detection. *Biol. Cybern.* 72: 261–277.
- Longuet-Higgins HC, S FR, Prazdny K (1980) The interpretation of a moving retinal image. *Proc. R. Soc. Lond.: B-Biol. Sci.* 208: 385–397.
- Meese TS, Harris SJ (2002) Spiral mechanisms are required to account for summation of complex motion components. *Vision Res.* 42: 1073–1080.
- Morrone MC, Burr DC, Vaina LM (1995) Two stages of visual processing for radial and circular motion. *Nature* 376: 507–509.

- Morrone MC, Tosetti M, Montanaro D, Fiorentini A, Cioni G, Burr DC (2000) A cortical area that responds specifically to optic flow, revealed by fMRI. *Nat. Neurosci.* 3: 1322–1328.
- Perrone JA (1992) Model for the computation of self-motion in biological systems. *J. Opt. Soc. Am. A* 9: 177–194.
- Perrone JA, Stone LS (1994) A model of self-motion estimation within primate extrastriate visual cortex. *Vision Res.* 34: 2917–2938.
- Rieger JH, Lawton DT (1985) Processing differential image motion. *J. Opt. Soc. Am. A* 2: 354–359.
- Schaafsma SJ, Duysens J (1996) Neurons in the ventral intraparietal area of awake macaque monkey closely resemble neurons in the dorsal part of the medial superior temporal area in their responses to optic flow patterns. *J. Neurophysiol.* 76: 4056–4068.
- Siegel RM, Read HL (1997) Analysis of optic flow in the monkey parietal area 7a. *Cereb. Cortex* 7: 327–346.
- Snowden RJ, Milne AB (1996) The effects of adapting to complex motions: Position invariance and tuning to spiral motions. *J. Cogn. Neurosci.* 8: 412–429.
- Sundareswaran V (1992) A fast method to estimate sensor translation. In: G Sandini, ed. *Computer Vision—ECCV '92 Second European Conference on Computer Vision*. Italy, Springer-Verlag, pp. 253–257.
- Vaina LM (1998) Complex motion perception and its deficits. *Curr. Opin. Neurobiol.* 8: 494–502.
- Vaina LM, Rushton SK (2000) What neurological patients tell us about the use of optical flow. *Int. Rev. Neurobiol.* 44: 293–313.
- Warren W, Morris M, Kalish M (1988) Perception of translational heading from optical flow. *J. Exp. Psychol. Hum. Percept. Perform* 14: 646–660.
- Zemel RS, Sejnowski TJ (1998) A model for encoding multiple object motions and self-motion in area MST of primate visual cortex. *J. Neurosci.* 18: 531–547.